

Three-Dimensional Resistivity vs. Depth Profiling for Advanced Characterization of the Lithium-Ion Battery Solid Electrolyte Interphase

Caleb Stetson, Yanli Yin, Andrew G. Norman, Nathan R. Neale, Chun-Sheng Jiang, Chunmei Ban, Steven C. DeCaluwe, and Mowafak M. Al-Jassim

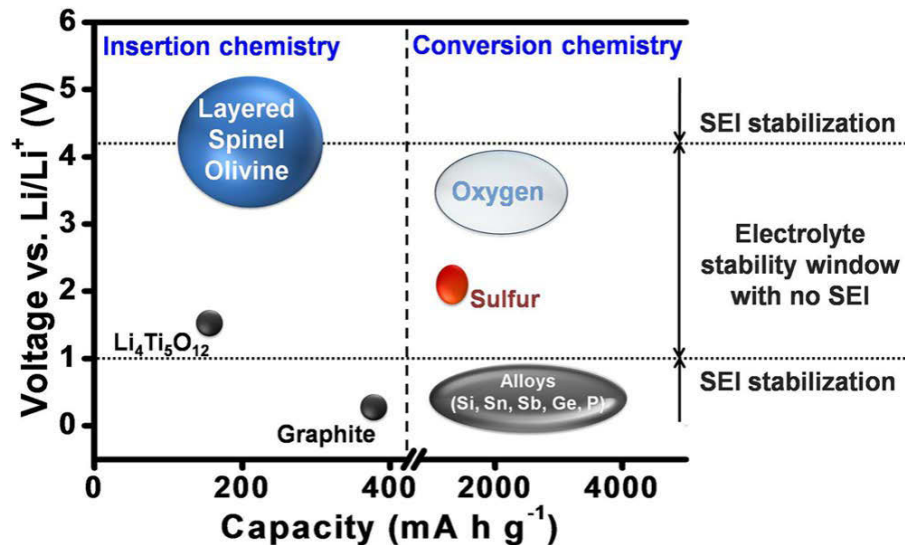
236th ECS Meeting

October 13-17, 2019

Atlanta, Georgia

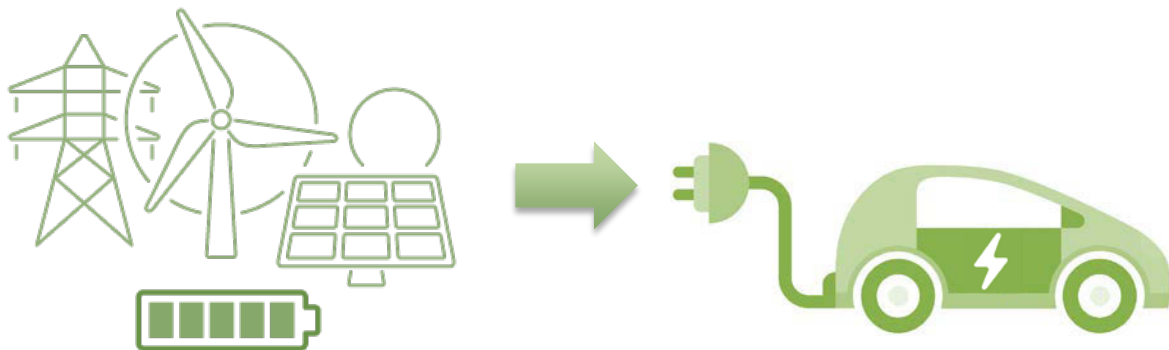
Next Generation Anode Materials for Lithium-Ion Batteries: Graphite vs. Silicon

- Si has an order of magnitude improvement in theoretical capacity over graphite
- Increased battery capacity could advance:
 - Renewable energy production and stationary storage
 - Electric vehicle grid integration



Capacity and voltage ranges for cathode and anode materials

Manthiram, A. *ACS Cent. Sci.*, 3, 2017.

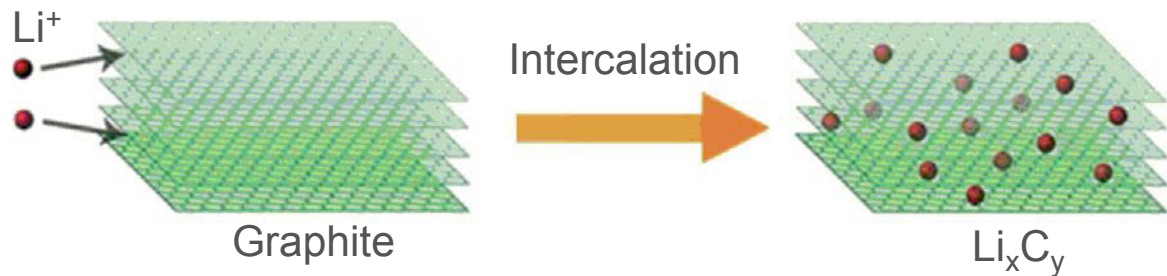


Renewable Energy & Grid Storage

Electric Vehicles

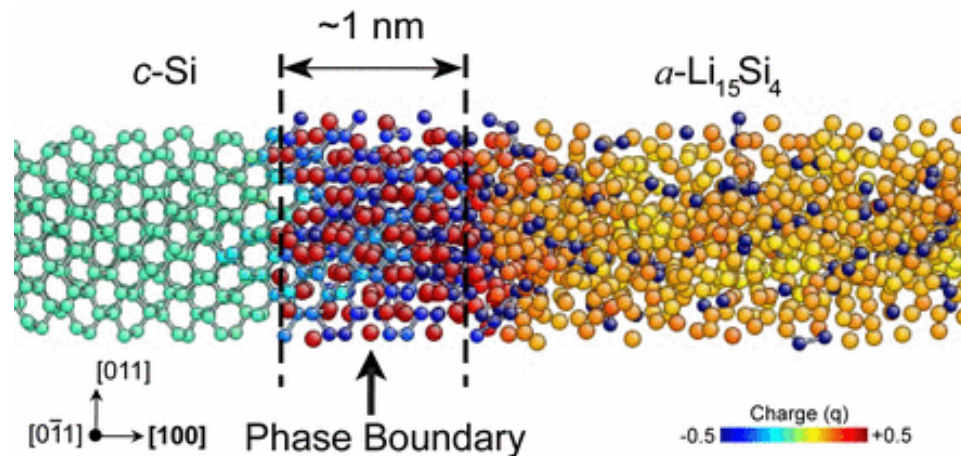
Lithium-Ion Battery Lithiation Mechanism: Graphite vs. Silicon

- In graphite anodes, Li^+ intercalates
- In Si anodes, Li^+ alloys with Si
- Greater relative expansion of Si anodes due to lithiation poses a challenge to anode stability and solid electrolyte interphase (SEI) passivation



Lithium intercalation in graphite

Huang, H., Xia, Y., Tao, X., Du, J., Fang, J., Gana, Y., Zhang, W. *J. Mater. Chem.*, 22. 2012.

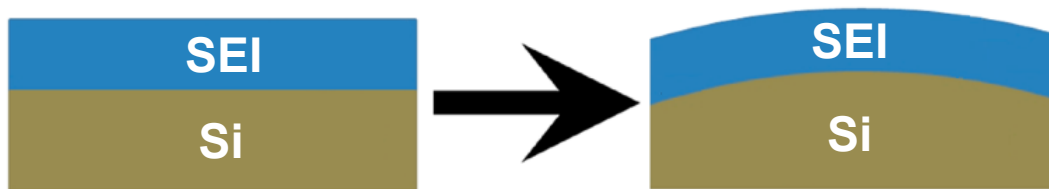
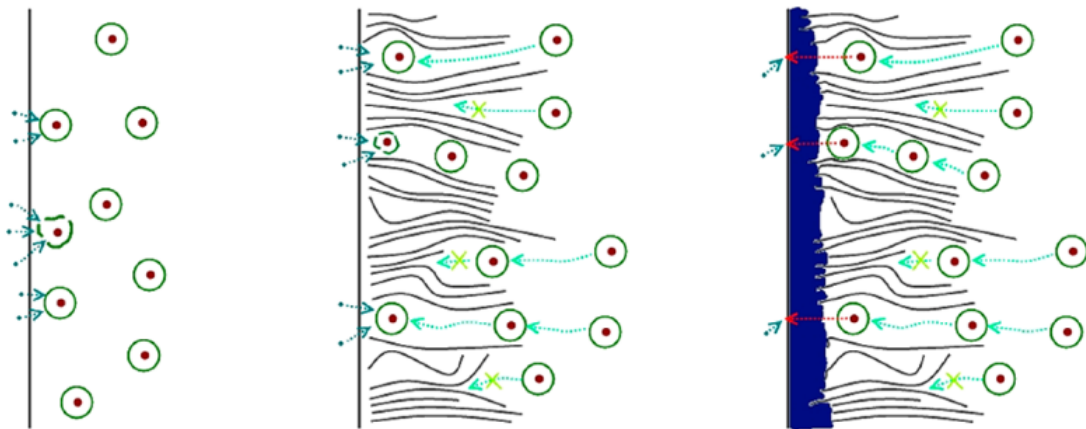


Lithium bonding in crystalline silicon.

Kim, S.P., Datta, D., Shenoy, V. *J Phys Chem C*, 118 (31). 2014.

Solid Electrolyte Interphase (SEI) on Si Anodes

- SEI forms from electrolyte reduction
- SEI is critical to maintaining anode passivation
 - Prevents further electrolyte decomposition
- A well-performing SEI must be:
 - Electronically resistive
 - Ionically conductive
 - Stable for an operating temperature range

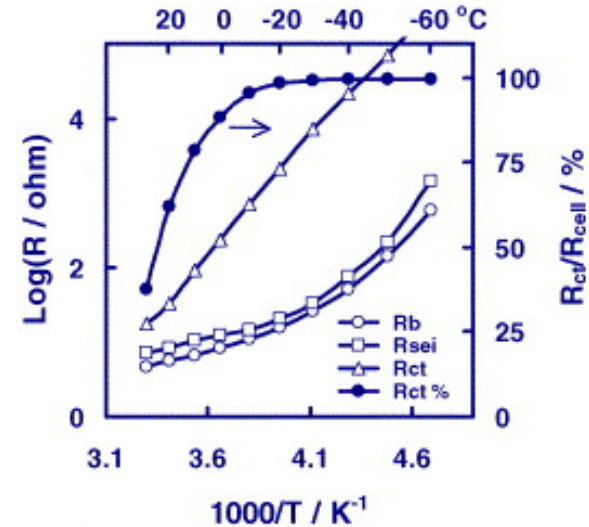
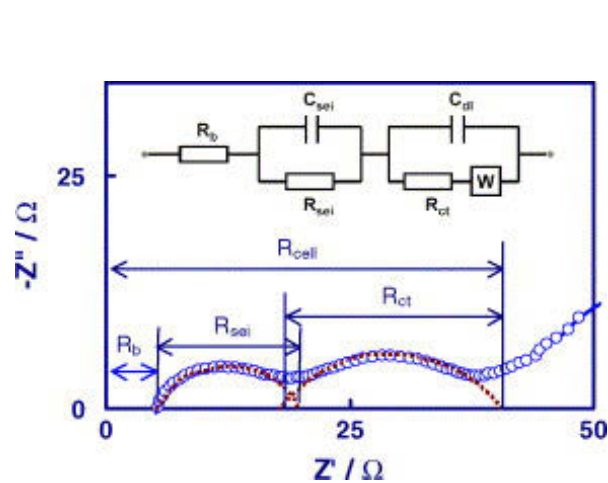


SEI formation on Silicon

Tokranov, A., Sheldon, B.W., Li, C., Minne, S., Xiao, X.
ACS Appl. Mater. Interfaces, 6. 2016.

Characterization of Electronic Resistivity of SEI

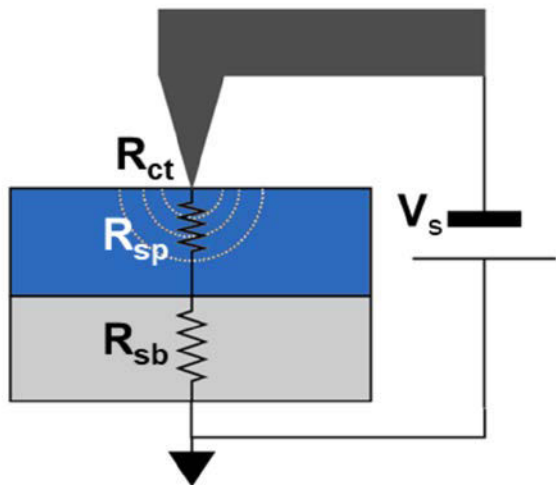
- Traditionally, electrochemical impedance spectroscopy (EIS) is used to measure electronic properties of SEI within a cell
- However, measured SEI resistance is representative of the entire structure
- Previously, a nanoscale characterization tool capable of measuring SEI electronic properties has been lacking



EIS Characterization of R_{SEI}

Zhang, S. S.; Xu, K.; Jow, T. R., Electrochemical impedance study on the low temperature of Li-ion batteries. *Electrochimica Acta* **2004**, 49 (7), 1057-1061.

Characterization of SEI: 3-D Resistivity vs. Depth Profiling with Scanning Spreading Resistance Microscopy (SSRM)



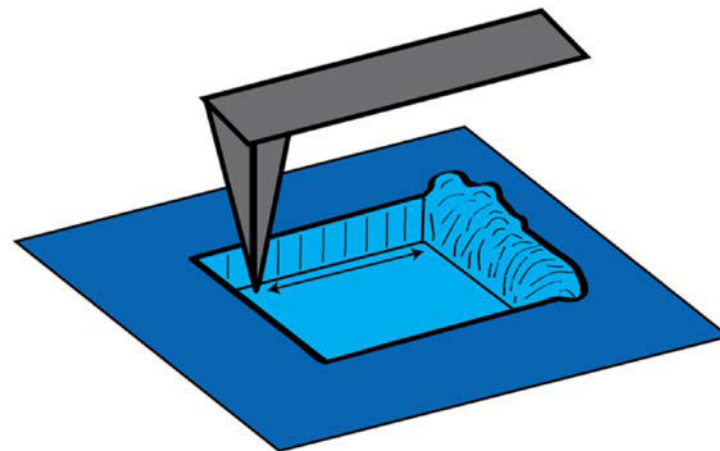
SSRM Schematic

R_{ct} : contact resistance

R_{sp} : spreading resistance

R_{sb} : sample to back contact resistance

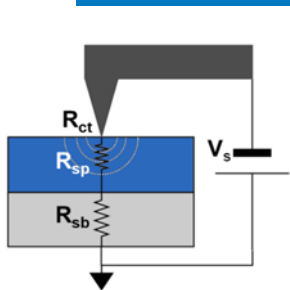
$$R_{ct} \gg R_{sp}$$



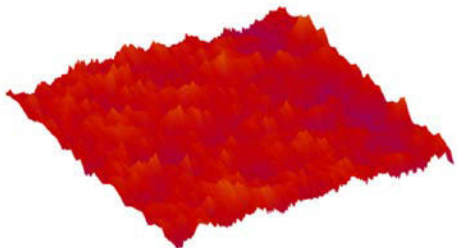
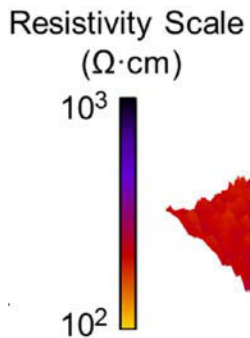
Conceptual illustration of 3-D resistivity vs. Depth profiling into SEI

Stetson, C., Yoon, T., Coyle, J., Nemeth, W., Young, M., Norman, A., Pylypenko, S., Ban, C., Jiang, C.S., Al-Jassim, M., Burrell, A. *Nano Energy*, 55. 2019.

Characterization of SEI: 3-D Resistivity vs. Depth Profiling with Scanning Spreading Resistance Microscopy (SSRM)

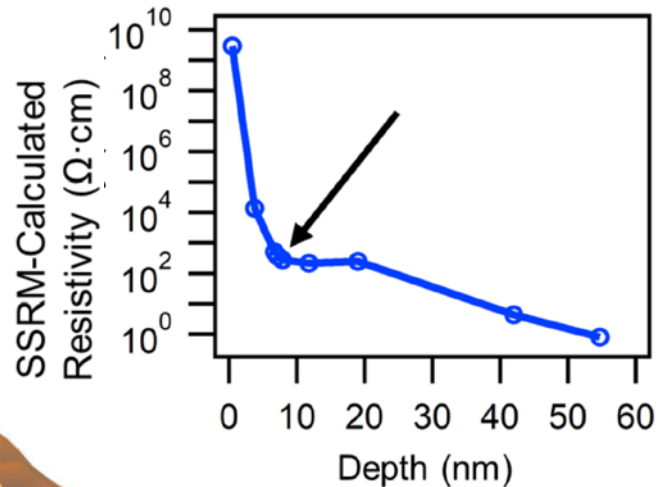
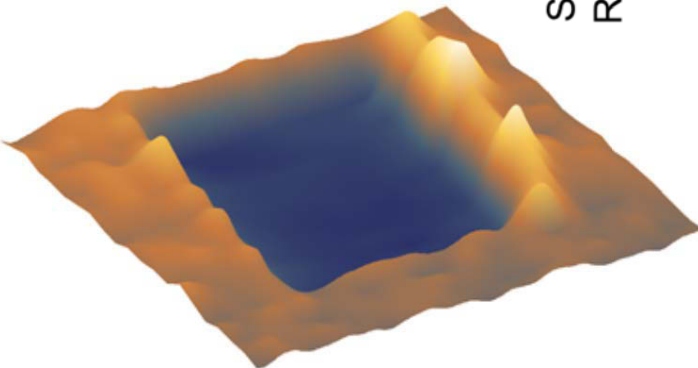


Height Map
(low probe force)



Resistivity Map
(intermediate probe force)

Height Scale (nm)

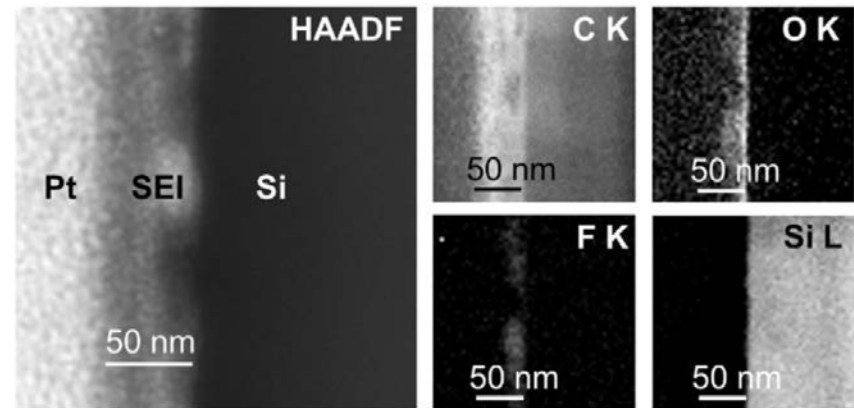
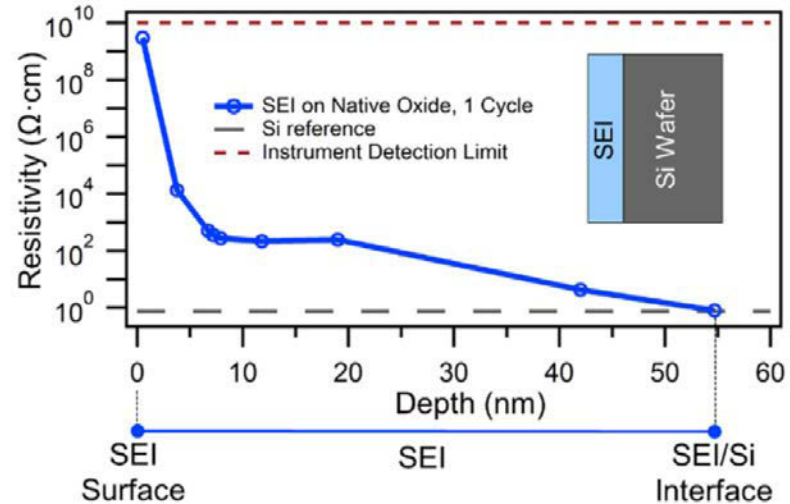


Stetson, C., Yoon, T., Coyle, J., Nemeth, W., Young, M., Norman, A., Pylypenko, S., Ban, C., Jiang, C.S., Al-Jassim, M., Burrell, A. *Nano Energy*, 55. 2019.

Comparative Nanoscale Characterization: SSRM 3-D Resistivity vs. Depth Profiling and STEM EELS

- Higher resistivity superficial SEI detected with SSRM shows correlation with organic-rich superficial SEI
- Lower resistivity SEI at the Si interface correlates with F and O, indicative of inorganic SEI composition (LiF, Li₂O)
- SSRM and STEM show good agreement for total SEI thickness

- Coin Cell, half cell vs. Li/Li⁺
- Native SiO_x terminated Si wafer
- Gen2
Electrolyte: EC:EMC (3:7 by wt.) + 1.2M LiPF₆
- 22 μA cm⁻² fixed current density, 5 h half cycle, 1 Cycle



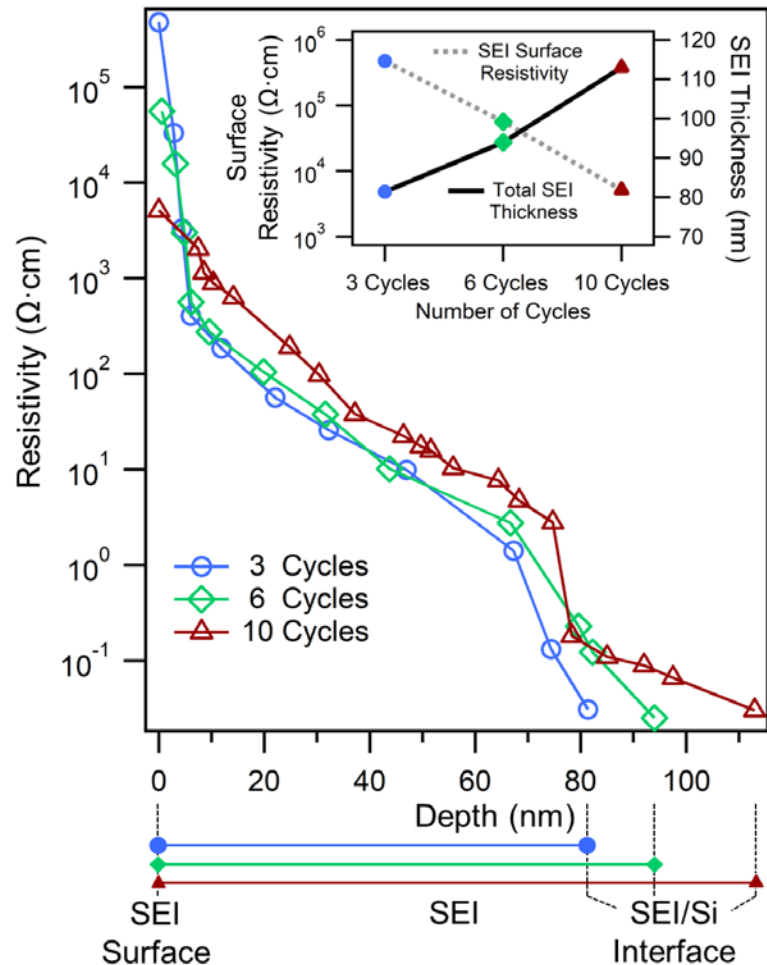
Stetson, C., Yoon, T., Coyle, J., Nemeth, W., Young, M., Norman, A., Pylypenko, S., Ban, C., Jiang, C.S., Al-Jassim, M., Burrell, A. *Nano Energy*, 55. 2019.

Studies into SEI Formation and Evolution

SEI Evolution through Early Cycling

- SEI shows an increase in thickness from 3→6→10 cycles
- SEI Surface resistivity decreases from 3→6→10 cycles
- Suggestive of a loss of segregation in SEI components during SEI “breathing”

- Coin Cell, half cell vs. Li/Li^+
- Native SiO_x terminated Si wafer
- Gen2 Electrolyte: EC:EMC (3:7 by wt.) + 1.2M LiPF_6
- $22 \mu\text{A cm}^{-2}$ fixed current density, 2 h half cycle

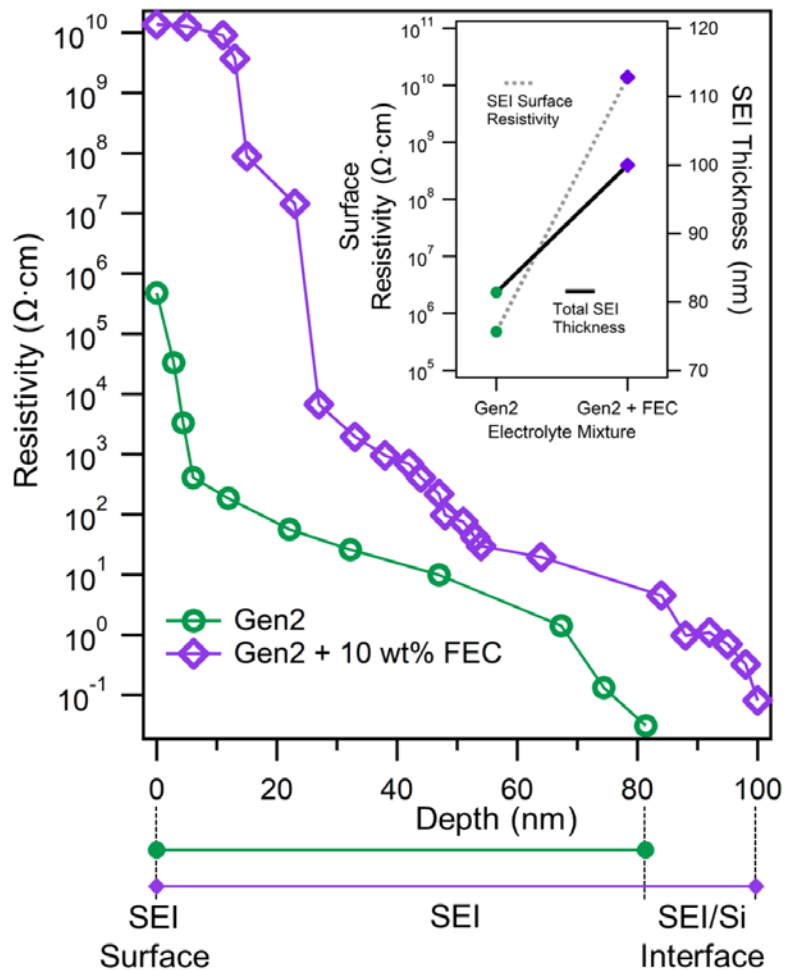


Stetson, C., Yoon, T., Coyle, J., Nemeth, W., Young, M., Norman, A., Pylypenko, S., Ban, C., Jiang, C.S., Al-Jassim, M., Burrell, A. *Nano Energy*, 55. 2019.

Effect of Electrolyte Additive on SEI Formation

- SEI formed with FEC additive shows a greater thickness, with higher electronic resistivity throughout
- High electronic resistivity of SEI grants improved anode passivation, partially explaining cycling performance improvement of FEC additive in lithium-ion batteries

- Coin Cell, half cell vs. Li/Li^+
- Native SiO_x terminated Si wafer
- Gen2 Electrolyte: EC:EMC (3:7 by wt.) + 1.2M LiPF_6
- $22 \mu\text{A cm}^{-2}$ fixed current density, 2 h half cycle,

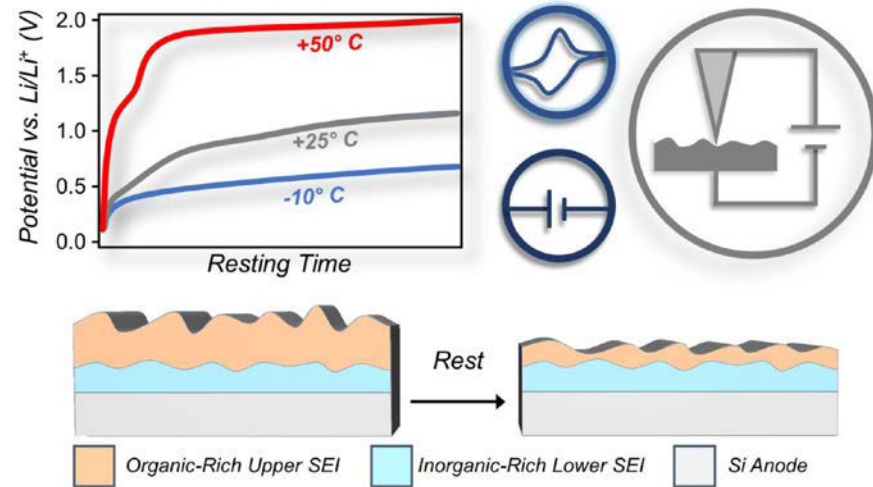


Stetson, C., Yoon, T., Coyle, J., Nemeth, W., Young, M., Norman, A., Pylipenko, S., Ban, C., Jiang, C.S., Al-Jassim, M., Burrell, A. *Nano Energy*, 55. 2019.

Studies into Equilibrated SEI: SEI Solubility

Temperature-Dependent Solubility of SEI

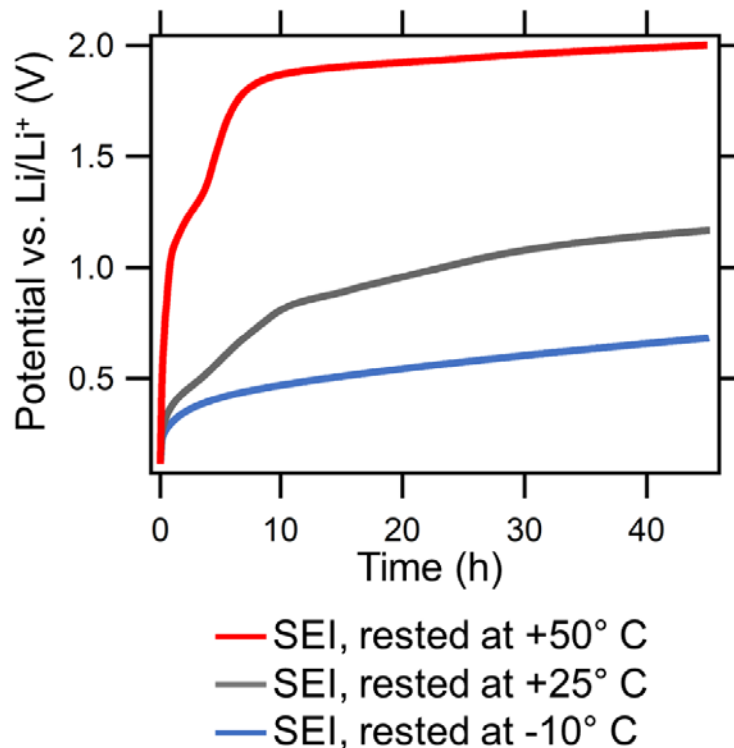
- Through cycling protocols that limit lithiation of Si, SEI at later stages of equilibration can be evaluated independently of heterogeneity induced by Si expansion
- Distinct resting protocols, at different temperatures within the operational range of lithium-ion batteries, permits study of the temperature-dependent solubility/stability of SEI



Stetson, C., Yin, Y., Jiang, C.S., DeCaluwe, S.C., Al-Jassim, M., Neale, N.R., Ban, C., Burrell, A. *ACS Energy Lett.*, Under Review.

Temperature-Dependent Solubility of SEI

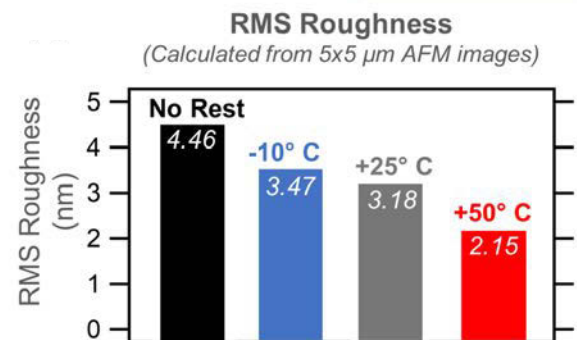
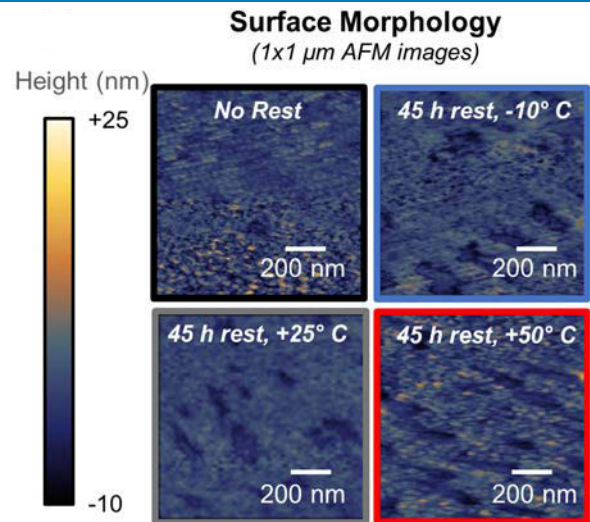
- During cell rest, OCV increases at faster rates at higher temperatures, indicative of temperature-dependent kinetics and thermodynamics
- After cell rest, SEI was investigated with AFM and 3-D Resistivity vs. Depth Profiling to measure changes to SEI during resting at different temperatures



Stetson, C., Yin, Y., Jiang, C.S., DeCaluwe, S.C., Al-Jassim, M., Neale, N.R., Ban, C., Burrell, A. *ACS Energy Lett.*, Under Review.

Temperature-Dependent Solubility of SEI

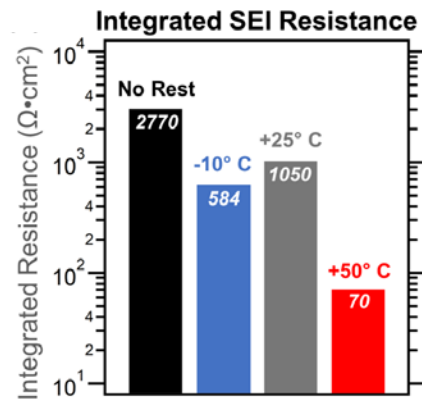
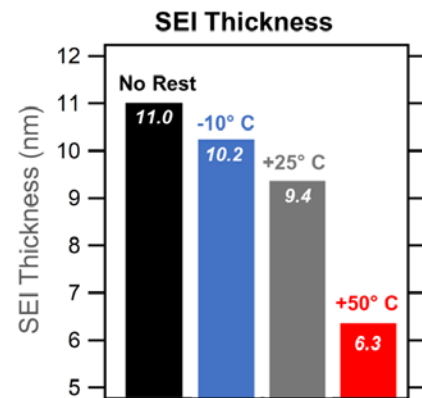
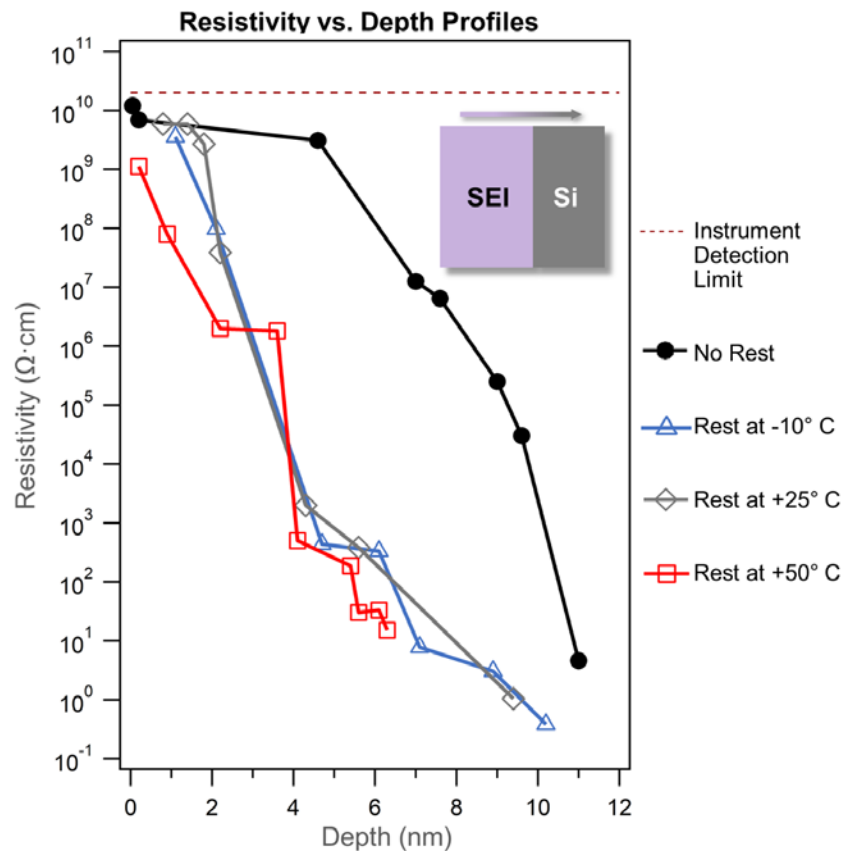
- AFM morphology showed a decrease in surface roughness through resting
- Pitting morphology appeared in rested samples, visible in 1 x 1 μm AFM images



Stetson, C., Yin, Y., Jiang, C.S., DeCaluwe, S.C., Al-Jassim, M., Neale, N.R., Ban, C., Burrell, A. *ACS Energy Lett.*, Under Review.

Temperature-Dependent Solubility of SEI

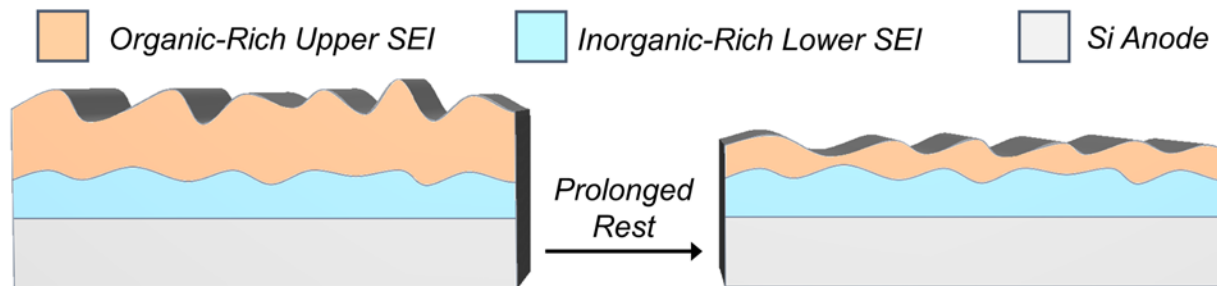
- A loss of resistive composition was observed in all rested samples
- Thickness also decreased during resting



Stetson, C., Yin, Y., Jiang, C.S., DeCaluwe, S.C., Al-Jassim, M., Neale, N.R., Ban, C., Burrell, A. *ACS Energy Lett.*, Under Review.

Temperature-Dependent Solubility of SEI: Conclusions

- AFM morphology showed a decrease in surface roughness through resting
- SSRM 3-D Resistivity vs. Depth profiles showed a decrease in thickness and resistivity
- These results suggest that the superficial SEI, rich in organic composition, selectively dissolves/decomposes during resting at higher temperatures



Stetson, C., Yin, Y., Jiang, C.S., DeCaluwe, S.C., Al-Jassim, M., Neale, N.R., Ban, C., Burrell, A. *ACS Energy Lett.*, Under Review.

Thank You

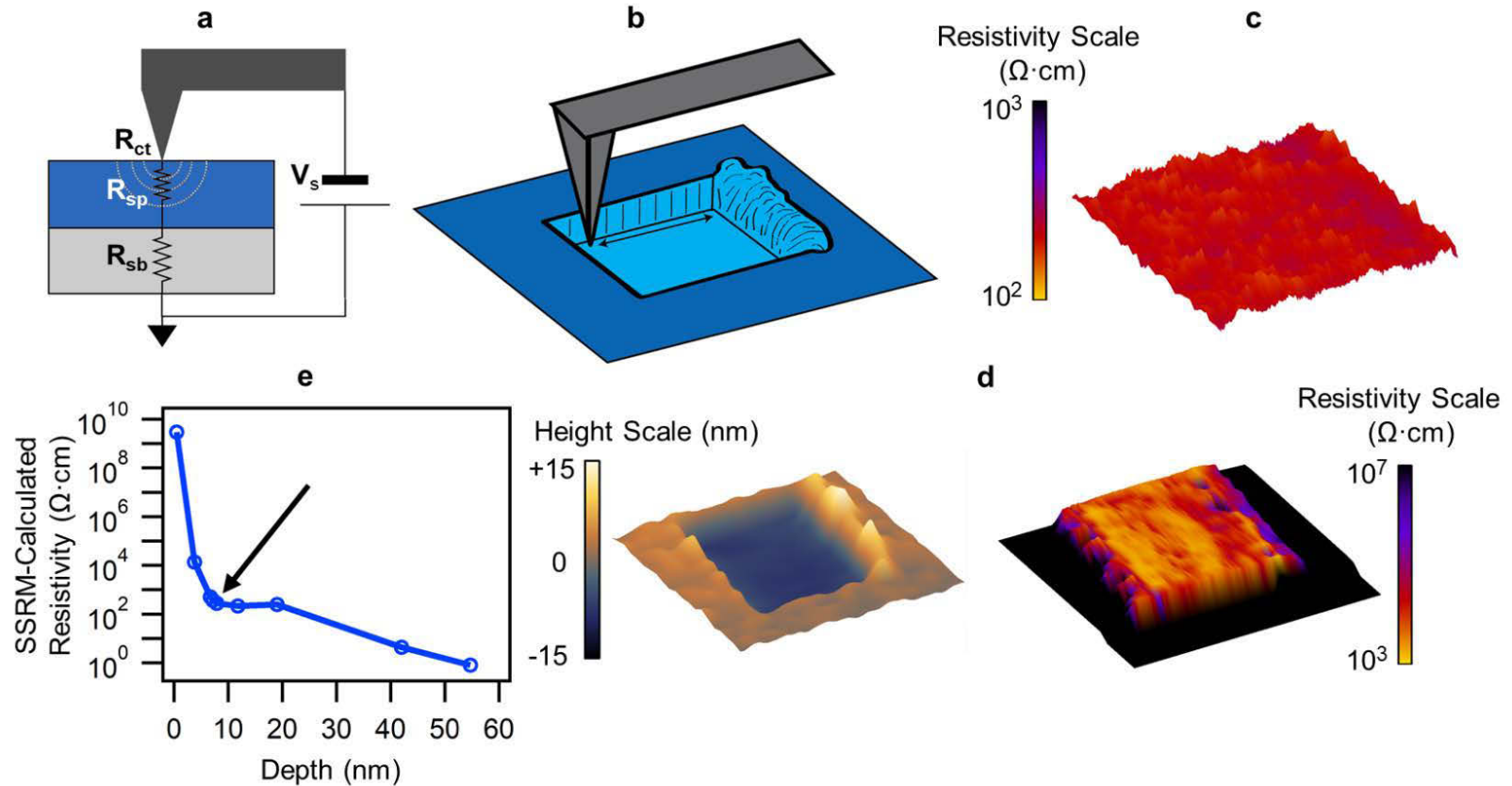
www.nrel.gov

NREL/PR-5K00-75167

This work was authored in part by the National Renewable Energy Laboratory, operated by Alliance for Sustainable Energy, LLC, for the U.S. Department of Energy (DOE) under Contract No. DE-AC36-08GO28308. Funding provided by the U.S. Department of Energy Office of Energy Efficiency and Renewable Energy Vehicle Technologies Office. The views expressed in the article do not necessarily represent the views of the DOE or the U.S. Government. The U.S. Government retains and the publisher, by accepting the article for publication, acknowledges that the U.S. Government retains a nonexclusive, paid-up, irrevocable, worldwide license to publish or reproduce the published form of this work, or allow others to do so, for U.S. Government purposes.



Reference Slides



Stetson, C., Yoon, T., Coyle, J., Nemeth, W., Young, M., Norman, A., Pylypenko, S., Ban, C., Jiang, C.S., Al-Jassim, M., Burrell, A. *Nano Energy*, 55. 2019.

Reference Slides

Stetson, C., Yoon, T., Coyle, J., Nemeth, W., Young, M., Norman, A., Pylypenko, S., Ban, C., Jiang, C.S., Al-Jassim, M., Burrell, A.
Nano Energy, 55. 2019.

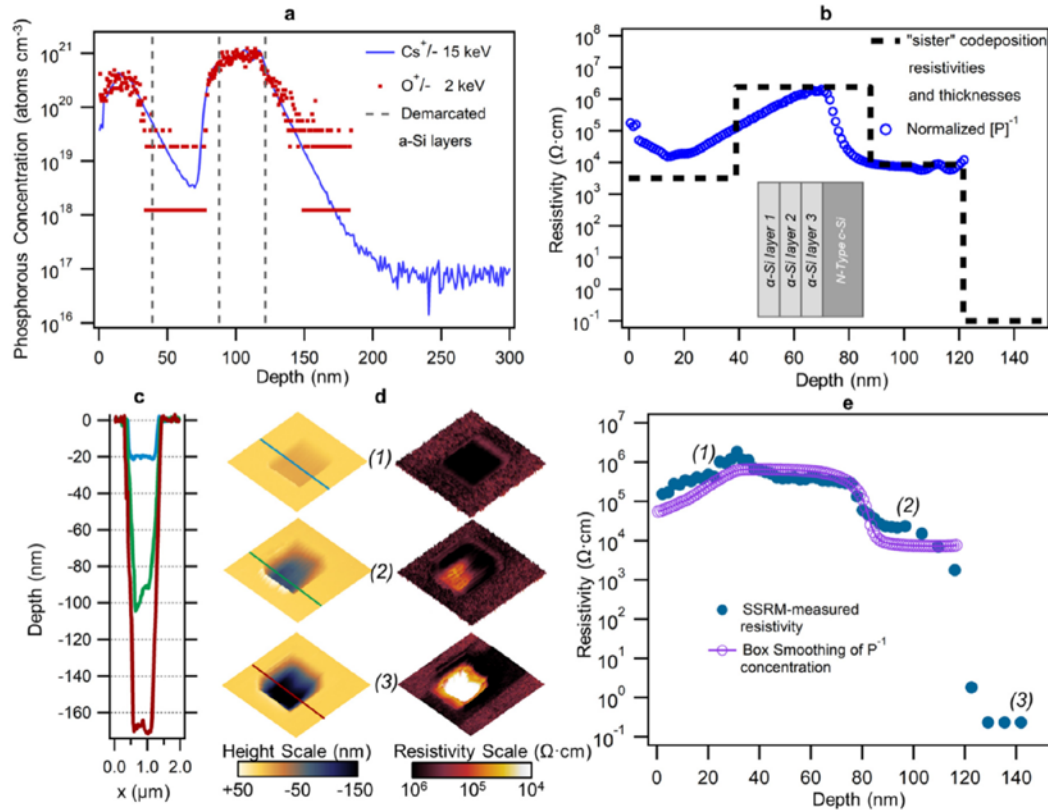


Fig. 3. SIMS and SSRM data for doped α -Si:H on c-Si reference sample. (a) Dynamic SIMS P-concentrations measured with cesium and oxygen sputtering at 15 keV and 2 keV, respectively. (b) Inverse P-concentration, normalized to highest bulk resistivity, measured on "sister" codeposition on glass. Sample schematic with thicknesses is shown in inset. (c) Line scans across overview height images captured during various stages of incremental SSRM profiling, showing three distinct depths within the structure. (d) $2 \times 2 \mu\text{m}$ height (left) and resistivity (right) overview images at three stages of incremental SSRM profiling, demonstrating contrast in electronic resistivities at different depths within the structure. (e) SSRM resistivity vs. depth profile for the sample. Box-smoothing of normalized inverse P-concentration data shows close agreement with SSRM data after smoothing to include 10 nm of previous points (to account for probe tip penetration) and 40 nm of subsequent points (to account for the sampling volume of the spreading resistance).